

Cyclic Behavior of Embedded Column-to-Foundation Connections in Circular CFST Columns: An Experimental and Numerical Study

Saleh Mohammad-Ebrahimzadeh-Sepasgozar^{a*}, Morteza Naghipour^{a,b}

^a Faculty of Civil Engineering, Babol Noshirvani University of Technology, Babol, Iran

ARTICLE INFO

Keywords:

Embedded connection
CFST column
Cyclic behavior
Axial load
Seismic performance
Energy dissipation

Article history:

Received 08 July 2025
Accepted 21 July 2025
Available online 01 August 2025

ABSTRACT

This study investigates the cyclic performance of embedded column-to-foundation connections in circular concrete-filled steel tube (CFST) columns through experimental testing and numerical simulations. While base-plate connections are commonly used in composite structures, embedding the column into the foundation provides notable advantages, including increased strength, stiffness, and ductility under seismic loading. Experimental results confirmed that embedded connections are capable of fully transferring axial and lateral loads. Failure primarily occurred through plastic hinge formation at the column base, with no evidence of brittle fracture or pull-out. Increasing the embedment depth (L_e) significantly enhanced flexural capacity, energy dissipation, and cyclic stability. An embedment depth equal to the column diameter ($L_e = D$) was sufficient to achieve full moment transfer, while deeper embedments ($L_e > 1.2D$) further improved hysteretic behavior and mitigated stiffness degradation at large displacements. The circular geometry of the column, combined with confinement from the surrounding concrete, generated an effective triaxial stress state (i.e., compressive stresses in all three directions) that enhanced mechanical interlock between the steel tube and the concrete core. Numerical simulations corroborated the experimental findings and provided additional insights into stress distribution, confinement effects, and shear transfer mechanisms. Increased friction and contact area within the interaction zone contributed to greater initial stiffness and improved post-yield strength. Parametric analyses revealed that an axial load ratio up to 0.2, particularly in conjunction with high-strength concrete, enhanced seismic performance. However, higher axial ratios (e.g., 0.3) led to local buckling and reduced ductility. For optimal seismic design, it is recommended to embed the column to a depth at least equal to its diameter and maintain the axial load ratio within the range of 0.1 to 0.2.

1. Introduction

Building structures must be capable of transferring both vertical (gravity) and lateral forces to the supporting elements. In most structural systems, the reinforced concrete foundation serves as the primary supporting component [1]. The column base connection is considered the most critical interface between the steel superstructure and the foundation. The performance of steel column base connection details is essential not only for transferring the imposed loads to the foundation but also for ensuring the temporary vertical stability of columns (without lateral bracing) during erection and wind loads encountered during construction. The placement of anchor bolts, as one of the key components for structural safety during erection and accurate positioning of the superstructure, is of vital importance and cannot be overlooked. Column base plates and their corresponding details typically represent the final elements to be designed, but the first to be installed during construction. Fig. 1 illustrates the typical components

* Corresponding author.

E-mail addresses: civil.sepasgozar@stu.nit.ac.ir (S. M. Ebrahimzadeh Sepasgozar).

<https://doi.org/10.22080/ceas.2025.29629.1027>

ISSN: 3092-7749/© 2025 The Author(s). Published by University of Mazandaran.

This article is an open access article distributed under the terms and conditions of the Creative Commons Attribution (CC-BY) license (<https://creativecommons.org/licenses/by/4.0/deed.en>)

How to cite this article: Ebrahimzadeh Sepasgozar, S. M., Naghipour, M. Cyclic Behavior of Embedded Column-to-Foundation Connections in Circular CFST Columns: An Experimental and Numerical Study. Civil Engineering and Applied Solutions. 2025; 1(3): 29–47. doi:10.22080/ceas.2025.29629.1027.



of a steel column base connection, including the base plate, anchor bars, stiffening gusset plates, welds, connection angles, and grout layer [2]. Many conventional steel base plates have sustained damage during major earthquakes, prompting revisions in design methodologies. Notable seismic events such as the 1978 Iso-Oshima and Miyagi-Ken-Oki earthquakes, as well as the 1995 Kobe earthquake, have highlighted these vulnerabilities.

Previous studies investigating steel column-to-foundation connections have primarily focused on evaluating stiffness, strength, and failure modes. Several notable contributions and research have been published in the literature in this field [3-7]. The widespread damage observed in steel base plates following the 1995 Kobe earthquake prompted Japanese researchers to revisit the design methodology of uncovered base connections. As a result, research efforts concentrated on connections that maintained their strength post-yielding to enhance seismic performance. Hitaka et al. [8], [9] focused specifically on improving the strength, stiffness, and ductility of exposed base connections. In 2004, Marson and Bruneau [10] examined the seismic response of circular CFST column base connections, highlighting the influence of tube cross-sectional geometry. Their specimens exhibited favorable hysteretic behavior and high energy dissipation capacity, with all specimens demonstrating good ductility.

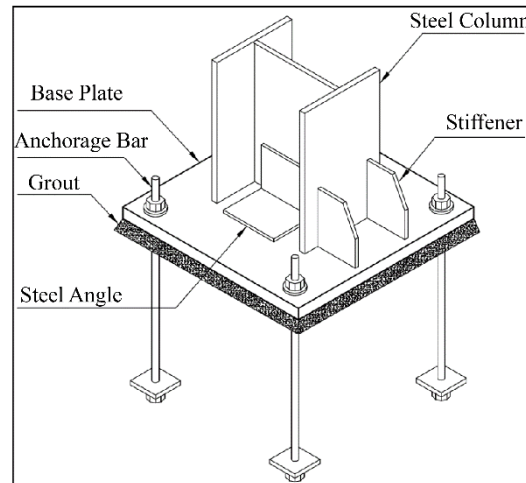


Fig. 1. Configuration of the base plate connection.

Zhang et al. [11] subjected CFST column base specimens encased in concrete to low-cycle seismic loading. Their findings revealed that low-cycle fatigue behavior strongly depended on the steel tube thickness. In 2010, Roeder Charles et al. [12] analyzed circular CFST columns under combined axial and bending loads. Their study presented an effective theoretical model for predicting the stiffness and strength of circular CFST columns, demonstrating that the plastic stress method offered a simple and efficient approach for assessing CFST behavior under combined loading. Between 2012 and 2013, Moon et al. [13], [14, 15] investigated circular CFST columns used in piles, piers, and bridge columns. Specimens were subjected to flexural loading in both experimental and numerical setups, and were evaluated for various diameter-to-thickness ratios. Later in 2013, Moon et al. [15] studied embedded circular CFST column-to-foundation connections under combined axial and flexural loads, followed by Lee et al. [16], who enhanced the punching shear resistance and ductility of foundations and connections using embedded shear-resisting elements. In 2016, Moon et al. [17] further conducted analytical evaluations of reinforced concrete column-to-steel pile connections. Their findings emphasized that embedment depth and the friction coefficient between the infilled concrete and steel pile had a significant impact on the seismic performance of bridge foundations.

While the seismic performance of CFST columns and connections has been rigorously studied in Iran over recent years, limited attention has been given to embedded base connections of CFST members. Despite past research efforts, current structural design literature lacks comprehensive guidelines for embedded base connection design. Furthermore, leading design codes, including Iran's national building regulations, part 10 [18] do not sufficiently address embedded base connection detailing, nor provide modern design provisions. Several studies [19-22] addressed the seismic response of exposed connections between the CFST column and foundation under cyclic loading. The findings demonstrated that the exposed connection failed in the form of concrete crushing, together with the yielding of the base plate and anchor bolt. Many investigations [23-27] examined the lateral shear capacity and load transfer mechanism in the column to foundation connections. The results demonstrated that despite a slight increase in the capacity to carry lateral loads, the energy absorption capacity increased significantly. Other similar research has been conducted on prefabricated column connections to the foundation with sockets, and the results of these studies also demonstrated that when the embedded depth of the column is sufficiently large, the connected members can present suitable hysteresis performance and ultimate failure mode [28, 29].

Other studies by Wang et al. [30] and Zhang et al. [31] on connections of the precast pier to the foundation or cap beam showed that when the embedded depth was 1.13 to 1.5 times the column diameter, plastic damage was concentrated at the bottom of the column. Si et al. [32] and Zhang et al. [33] investigated a novel connection between CFST column-RC footing with shear keys or socket reinforcement and found that the socket depth, longitudinal reinforcement ratio, and axial load ratio significantly affected the mechanical performance of socket connections compared with other parameters. The results demonstrated that damage to specimens was often concentrated at the base of the columns, and the loading capacity slightly increased.

This study aims to experimentally and numerically evaluate the cyclic performance of CFST column-to-foundation embedded

connections. The focus lies in identifying and characterizing damage modes observed in specimens under cyclic loading, and tracking relative drift progression until complete failure. Failure scenarios include pull-out, tube yielding, local buckling, initial tearing, and full rupture.

2. Experimental program

2.1. Details of specimens

The experimental investigation was conducted on a circular concrete-filled steel tube (CFST) column embedded in a reinforced concrete foundation. The total height of the column from the top surface of the foundation to the point of lateral load application was 1200 mm. The outer diameter of the steel tube was 240 mm, with a wall thickness of 3.17 mm. The foundation block was constructed with dimensions of 1200 mm in length, 600 mm in width, and 400 mm in height.

The foundation was reinforced with longitudinal deformed bars of 16 mm diameter spaced at 100 mm, while transverse reinforcement was provided using 10 mm diameter stirrups at 100 mm spacing. In the embedded configuration, the bottom end of the CFST column was welded to a circular steel plate (ring-shaped) to ensure uniform transfer of axial and shear forces between the steel tube and the foundation concrete. Fig. 2 presents the construction details of the column-foundation assembly.

The reference specimen used in this study was constructed without internal stiffeners, and the embedment length of the steel tube into the foundation was designed as 1.2 times the outer diameter of the column (1.2D). This specimen served as the baseline for evaluating the structural performance of other configurations.

To ensure rotational and translational restraint of the foundation, a high-strength steel confinement frame was designed around it. Additionally, to mitigate potential stress concentrations in the corners and edges of the concrete foundation during loading, two U-shaped steel channels were welded to steel base members anchored to the laboratory floor. For applying cyclic lateral loads at the top of the column and preventing eccentricities or stress concentration during loading, two rigid steel plates were clamped to the column head using high-strength pre-tensioned bolts. Furthermore, to apply constant vertical compression and avoid local crushing at the column top, sufficient reinforcements were incorporated around the column head based on the size of the hydraulic actuator and column diameter, ensuring adequate stiffness. The steel cap plate at the column top had dimensions of (to be specified). The steel cap plate at the column top had dimensions of 400 mm in length, 300 mm in width, and 20 mm in thickness. The effective specimen height was measured from the point of lateral load application down to the top surface of the foundation.

Prior to casting, preparatory steps included leveling the concrete formwork, positioning the steel tube, assembling the reinforcement cage, and placing the concrete mold. To achieve the required embedment depth during casting, four L-shaped steel bars welded to the column base were used to anchor the steel tube within the foundation. Concrete was poured in layers to ensure adequate compaction and complete cavity filling. Since self-compacting concrete (SCC) was used for both the foundation and the steel tube infill, mechanical vibration was not required.

2.2. Material properties

The concrete used for both the column infill and the reinforced concrete foundation was a self-compacting concrete (SCC) mix. The mix proportions are detailed in Table 1. The water content was 190 l/m³, with 790 kg/m³ of sand, 420 kg/m³ of cement, 114 kg/m³ of limestone powder, 805 kg/m³ of coarse aggregate, and 5.5 l/m³ of high-range water-reducing admixture (superplasticizer). In addition, six standard cube specimens (100 mm × 100 mm × 100 mm) and six standard cylindrical specimens (dimensions to be defined) were cast from the same SCC batch to determine the compressive strength at 7 and 28 days. The results of these compressive strength tests are summarized in Table 2 provides a summary of specimen details. All material parameters presented in the table are based on the average values obtained from standardized measurements, as per the relevant test standards [34], and are shown in Fig. 3. The mechanical properties of SCC were determined using standard tests. Cylindrical compressive strength was measured as 39.95 MPa, while the cube compressive strength reached 48.73 MPa. The modulus of elasticity (E_c) was calculated to be 29,705 MPa, and the splitting tensile strength was 2.72 MPa.

Table 1. Mix design proportions for self-compacting concrete (SCC).

Water (l/m ³)	Sand (kg/m ³)	Cement (kg/m ³)	Limestone powder (kg/m ³)	Coarse aggregate (kg/m ³)	Superplasticizer (l/m ³)
190	790	420	114	805	5.5

Table 2. Mechanical properties of SCC.

Test type	Cylinder compressive strength (MPa)	Cube compressive strength (MPa)	Elastic modulus E_c (MPa)	Tensile strength (MPa)
SCC	39.95	48.73	29,705	2.72

The steel tube used in the CFST column was characterized by a yield strength (f_y) ranging from 304.11 MPa to 312.54 MPa, with an average value of 308.43 MPa. The ultimate tensile strength (f_u) ranged between 388.48 MPa and 398 MPa, with an average of 392.34 MPa. For the stress-strain behavior of the steel tube, three dog-bone tests were conducted, and the average mechanical properties were calculated. The three curves are presented in Fig. 3. The ultimate strain at failure (ϵ_u) was recorded at approximately 26.72%, indicating significant ductility of the steel material. For the A3-grade reinforcement bars used in the foundation, the yield strength was reported as 420 MPa, the ultimate tensile strength was 600 MPa, and the ultimate strain was 24%.

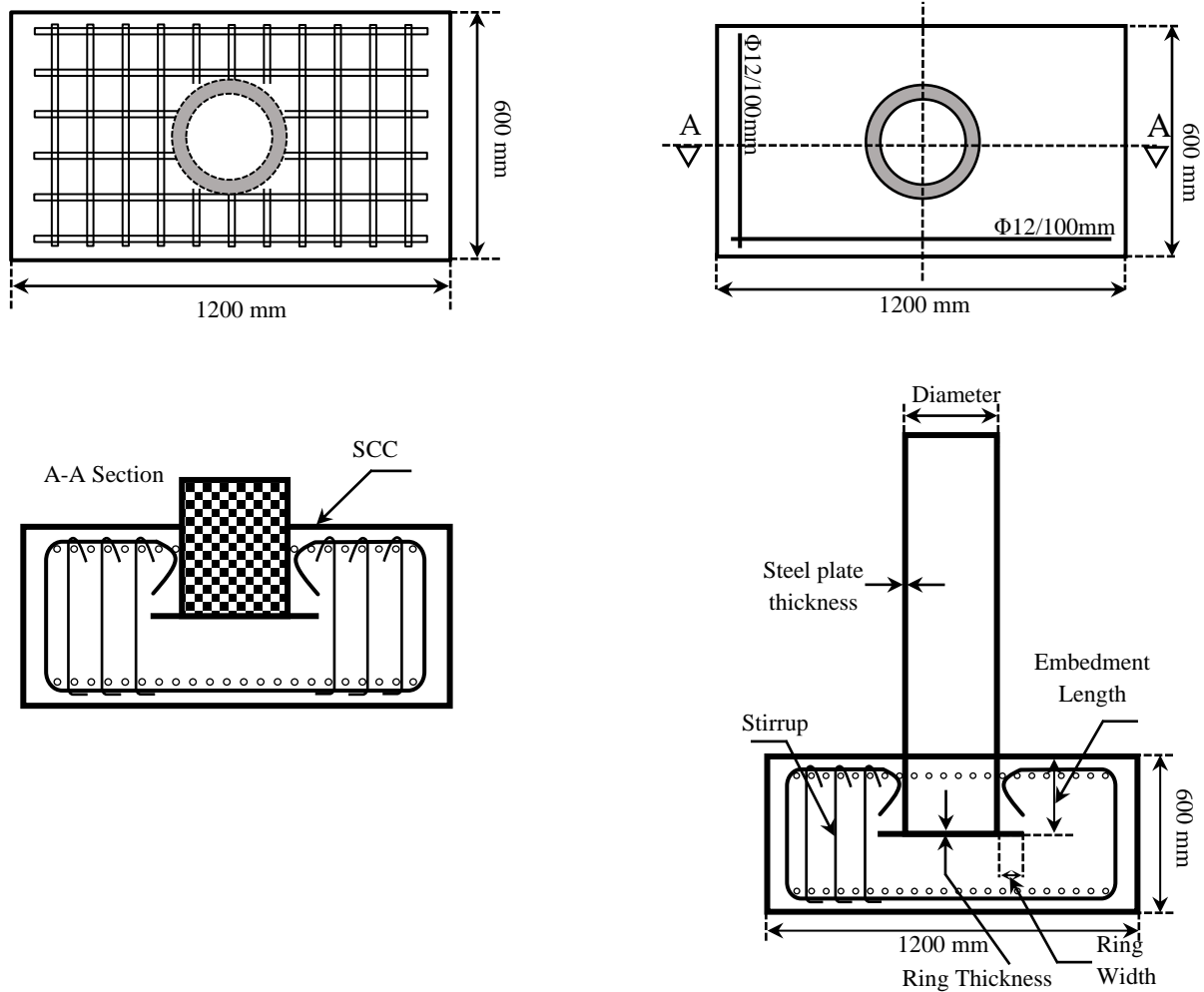


Fig. 2. Detailing and geometric dimensions of the CFST column-to-foundation connection in the embedded condition.

3. Experimental configuration and measurement systems

The tested column-to-foundation connection was subjected to a constant axial compressive load with a ratio of 0.2, alongside cyclic lateral displacement-controlled loading with increasing amplitude. The applied axial force ratio on the test specimen was calculated using the following formula.

$$n = p/p_n \quad (1)$$

In this equation, p represents the actual axial load applied to the top of the column, p_n is the nominal ultimate axial compressive bearing capacity, and n denotes the axial load ratio. The nominal compressive strength p_n of the circular CFST column was calculated in accordance with ACI 318 [34] provisions, as expressed by Eq. 2.

$$p_n = f_y \times A_s + 0.95f'_c \times A_c \quad (2)$$

In this equation, f'_c denotes the standard cylindrical compressive strength of concrete. According to ACI 318 [34] provisions, a conversion factor of 0.79 may be applied to estimate f'_c from compressive strength values obtained using standard cube specimens. The terms A_s and A_c represent the cross-sectional areas of the concrete core and steel tube, respectively. The slenderness ratio of the tested column (D/t) falls within the permissible range as defined by relevant design codes, including Iran's national building code [18], and AISC [35]. Following the experimental investigation, a parametric study was conducted, the details of which are presented in the finite element analysis section.

The experimental setup and the location of measurement instruments are depicted in Fig. 4. Axial loading was applied using a 1000 kN hydraulic jack, while the lateral cyclic load was imposed by another 1000 kN hydraulic jack. First, the axial load was applied at the column top to stabilize the specimen, followed by cyclic lateral displacement applied incrementally at the column head. To ensure accurate performance and alignment throughout the test, three hinged connections were incorporated:

- The first hinge was installed at the axial load application point atop the column,
- The second is at the interface of the lateral hydraulic jack and the column,
- And the third at the lateral jack's connection to the reaction frame.

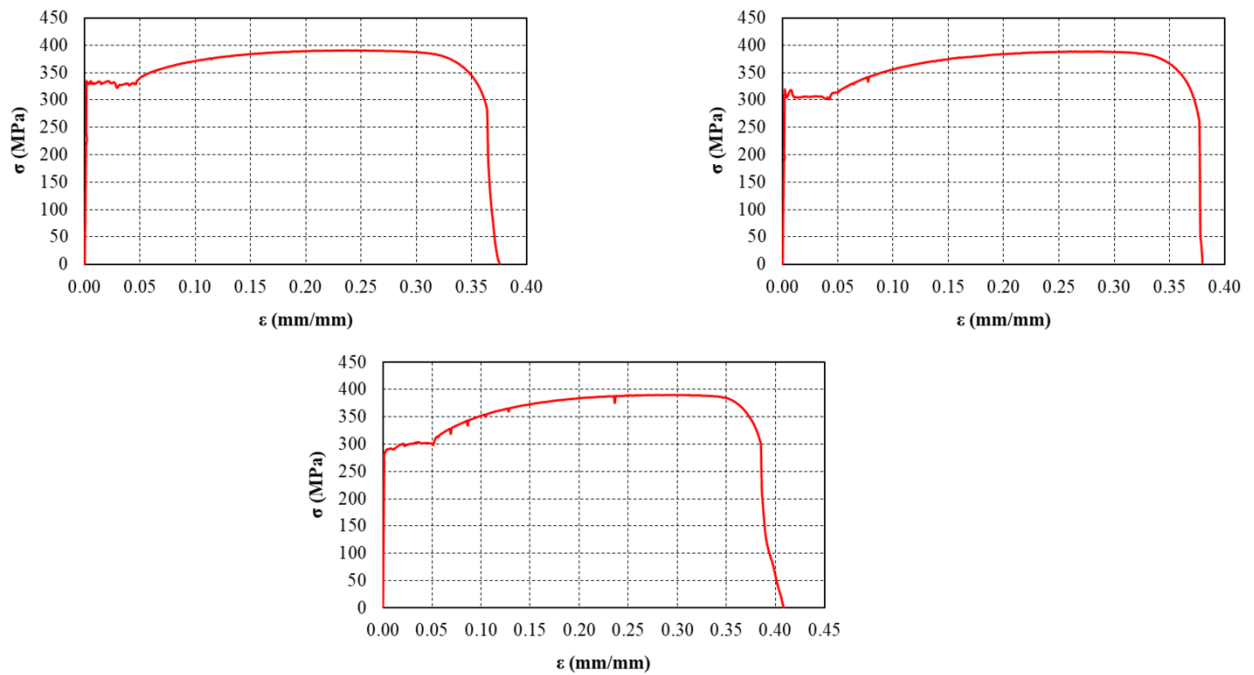


Fig. 3. Stress-strain curve from tensile test of steel tube.

Given that the axial jack was placed above the column, a sliding bearing was used at the interface between the jack and the reaction frame to eliminate unintended horizontal force components. Additionally, to prevent lateral slippage of the foundation during cyclic loading, steel bracing elements were anchored to the strong laboratory floor.

The connection was equipped with linear variable differential transformers (LVDTs) and strain gauges to monitor lateral displacement, support slippage, foundation uplift, and axial strains in the steel tube. The layout of the measurement instrumentation is illustrated in Fig. 4. Two LVDTs were positioned at the column head to measure lateral displacement at the point of load application. Displacement readings from these LVDTs were used to evaluate the hysteretic response of the specimen. Due to the potential for minor gaps between the loading head and the specimen surface, a sudden jump in LVDT values might occur. To counter foundation uplift and account for rotational movement, two additional LVDTs were installed at both ends of the foundation to capture any out-of-plane displacement, even with lateral bracing in place. To monitor localized buckling near the base of the column—a region especially prone to instability—two LVDTs were placed 50 mm above the foundation surface along the direction of lateral loading.

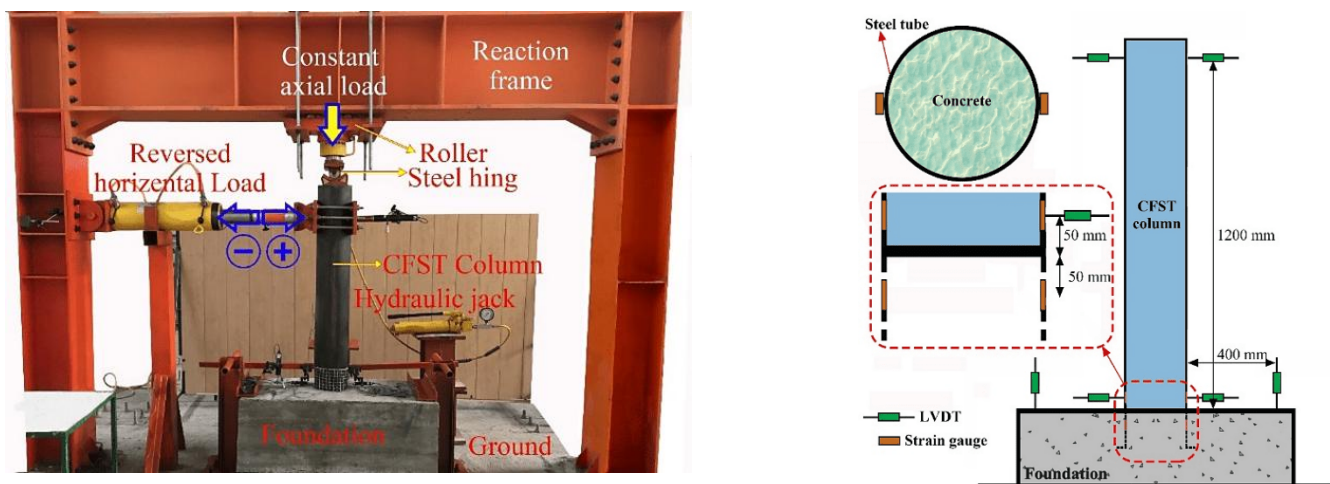


Fig. 4. Schematic of the rigid frame system: support conditions, loading actuators, and measurement systems.

A total of four strain gauges were attached to the steel tube. Two were located 50 mm above the foundation on the external tube surface, and the other two were embedded 50 mm below the surface within the foundation. All instrumentation positions are marked in Fig. 4.

4. Test procedure

Before the application of horizontal cyclic loading, the designated axial compressive load was applied to each specimen. In the initial stage, the axial load was increased at a constant rate of 2 kN/s using a 100 kN capacity axial hydraulic jack. The loading continued until the gap between the vertical loading jack piston and the top surface of the specimen was completely closed, ensuring that no eccentricity was introduced into the setup. Subsequently, a small lateral cyclic load was applied in several forward-reverse

cycles to stabilize the test system. Once the setup was fully stabilized, the specimen was subjected to low-cycle lateral loading. The reversed cyclic loading protocol was implemented based on the AISC standard [35], which specifies a displacement-controlled loading scheme with increasing amplitudes and predetermined cycle counts. The applied loading protocol, illustrated in Fig. 5, consisted of incremental displacement cycles. In the first 18 cycles, the applied displacements were maintained below the yield displacement (Δ_y) of the column. Specifically, the first 6 cycles were performed at 0.00375Δ , followed by 6 cycles at 0.005 , and then 6 cycles at 0.0075 . Next, the displacement amplitude was increased to 0.01 and applied over 4 cycles. Thereafter, loading was continued in two-cycle increments with increasing amplitudes until failure. In the subsequent stages, the first two cycles were carried out at 0.015 , followed by two cycles at 0.02 . The displacement ratio was then increased by 1% in each stage, with two cycles applied at each level. The cyclic loading was continued until the lateral load-carrying capacity of the system degraded to 85% of its peak lateral strength.

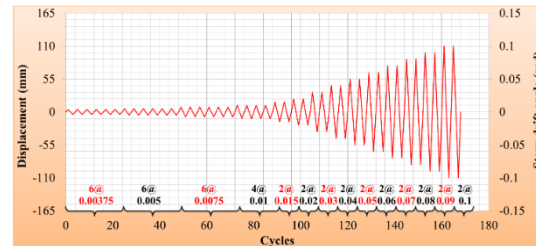


Fig. 5. Cyclic loading protocol.

5. Experimental observations

This section presents an evaluation of visual observations made during testing and the corresponding failure modes. In the tested specimens, plastic hinge formation was concentrated near the foundation at the base of the column. Fig. 6 presents a comparison of hysteresis curves obtained from experimental tests and numerical modeling. Table 3 summarizes the seismic performance parameters of the CFST specimens, comparing experimental and numerical results, including secant stiffness, yield load, maximum load, and yield displacement, ultimate displacement at 85% of peak load, ductility, and energy dissipation. The development of the plastic hinge led to outward bulging and local buckling of the steel tube, accompanied by concrete crushing within the steel tube. Local buckling at the column base was observed when the relative drift reached approximately 1.5% to 3%. At these drift levels, when the lateral load direction was reversed, local buckling in the tensile region tended to recover, while buckling persisted on the compression side. As lateral displacement increased further, local buckling intensified and became irreversible. Fig. 7 illustrates the observed failure patterns in the specimens. Due to the concentration of severe buckling and bulging at the column base, the plastic hinge was not distributed along the column height but was instead confined to a region approximately 25–75 mm above the foundation surface.

Visual inspection confirmed that the most critical damage zones were located within the column itself and not on the foundation surface, occurring at a measurable distance above the foundation. During cyclic testing, the specimens exhibited similar elastic behavior and maintained their ability to return to the original position after initial load applications. Upon entering the plastic stage and the onset of strain hardening, significant deformations appeared in the lower portion of the column near the connection zone. On the compression side, the steel tube showed gradual inward denting, while the tension side displayed signs of elongation and reduced curvature.

Columns with greater embedment depth exhibited smaller drift angles, indicating more stable and ductile flexural behavior. At peak lateral load, no signs of tensile failure or pull-out were observed at the column–foundation interface. The foundation surface also remained free of deep or through-thickness cracks, demonstrating the effectiveness of the embedded connection in transferring forces to the foundation. The use of bent or hooked reinforcement bars at the connection zone played a vital role in resisting tensile forces and maintaining connection integrity. Post-test inspection revealed that the plastic hinge had primarily formed close to the column base, indicating a ductile failure mechanism with gradual degradation. With increased embedment depth, this region shifted upward along the column, and a noticeable reduction in drift angle was recorded. Removal of the steel tube after testing showed minor vertical cracks on the surface of the concrete core and scattered horizontal cracks near the connection zone. These cracks were mainly concentrated near the shoulder or crown region of the cross-section, reflecting the concrete's response to cyclic loading. Overall, the use of embedded steel tubes in CFST columns proved effective in controlling localized deformations at the lower part of the column. However, the concrete core in some specimens exhibited relatively brittle behavior, underscoring the importance of incorporating internal reinforcement or appropriate transverse confinement to improve the cyclic performance of the column.

Table 3. Comparison of seismic performance parameters between experimental and numerical CFST specimens.

Specimen	Secant Stiffness	Yield Load	Maximum Load	Yield Displacement	Ultimate Displacement at 85% Peak Load	Ductility	Energy Dissipation
	K (kN/mm)	P_y (kN)	P_{max} (kN)	δ_y (mm)	δ_u (kN)	μ	E (kN.mm)
CCFC-Exp.	5.01	75.81	84.95	16.95	68.63	4.05	65472.88
CCFC - ABAQUS	5.33	78.80	86.72	16.27	69.38	4.27	68918.83
Percentage Difference	-6.36	-3.95	-2.09	4.01	-1.10	-5.32	-5.26

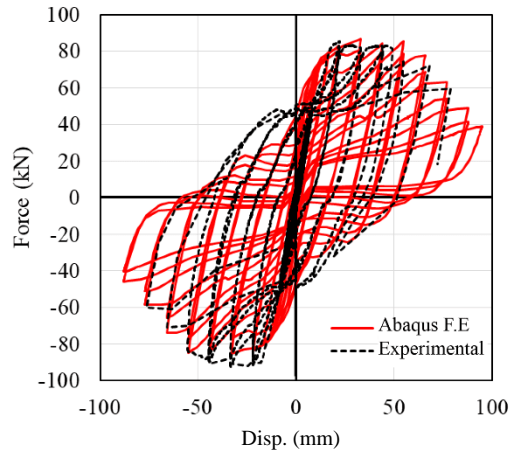
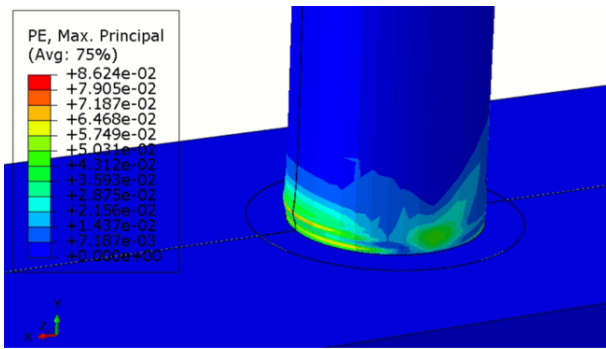


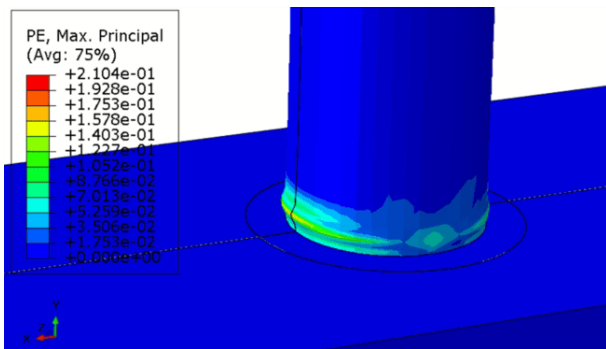
Fig. 6. Comparison of hysteresis curves: experimental vs. numerical model.

6. Numerical modeling

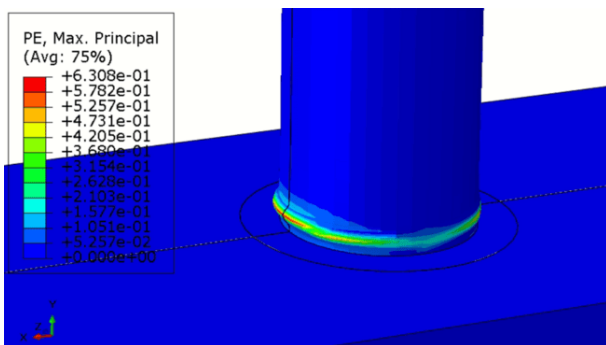
To investigate the nonlinear and cyclic behavior of embedded connections in circular concrete-filled steel tube (CFST) column foundations, the finite element software ABAQUS was employed. The finite element model comprised composite CFST columns, a reinforced concrete foundation, and the embedded connection zone. To improve computational efficiency and reduce analysis time, geometric symmetry with respect to the loading axis was utilized, and a half-symmetric model was developed accordingly.



(a)



(b)



(c)

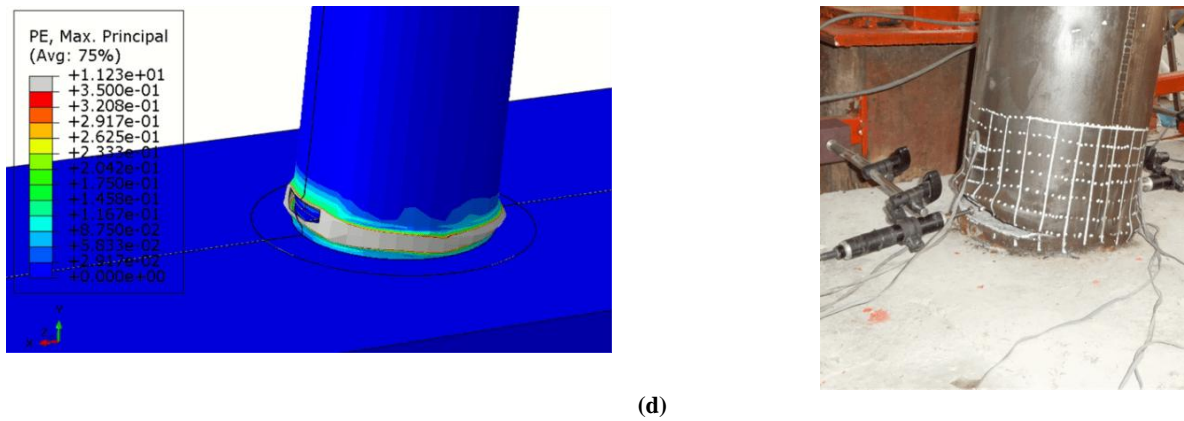


Fig. 7. Comparison of experimental and simulated damage states (cracking, yielding, and buckling) at incremental drift ratios: (a) 2%, (b) 4%, (c) 6%, (d) 8%.

The geometric model incorporated three types of elements: 8-node solid elements (C3D8R) for concrete, 4-node shell elements (S4R) for the steel tube, and 2-node truss elements (T3D2) for the reinforcement bars. To ensure analytical accuracy while maintaining numerical stability, a uniformly structured meshing scheme was adopted. A mesh size of 90 was assigned to the column and foundation components, while the reinforcement zone was modeled using a finer mesh size of 12. Table 4 presents the final meshing specifications.

In the model, the column–foundation interface was defined using hard contact in the vertical direction, while tangential behavior was governed by the Coulomb friction model with a friction coefficient of 0.3. Reinforcement bars were embedded within the concrete using the “Embedded Region” constraint to prevent relative slip between the reinforcement and surrounding concrete. Boundary conditions were applied as fully fixed (encastre) at the bottom of the foundation. Lateral loading was imposed as displacement-controlled at the column top in the horizontal direction, while vertical (gravity) loading was uniformly distributed and applied to both the concrete core and the steel tube. The numerical simulation was carried out using the Static, General analysis step in ABAQUS, which is well-suited for replicating quasi-static experimental procedures.

6.1. Material behavior models

To simulate concrete behavior under cyclic loading, the Concrete Damaged Plasticity (CDP) model was employed. The model parameters included a dilation angle of $\varphi = 30^\circ$, a biaxial-to-uniaxial compressive strength ratio $\beta = 1.16$, a ratio of the second deviatoric stress invariant in tension to compression $K = 0.667$, a viscosity parameter $\mu = 0.005$, and eccentricity $e = 0.1$. The Poisson's ratio for concrete was assumed to be 0.22. In the concrete model, the compressive stiffness recovery was set to 0.6, and tensile stiffness recovery was assumed to be zero to prevent regaining tensile stiffness after cracking. The nonlinear behavior of the steel tube and reinforcement bars was modeled using a bilinear kinematic hardening model with isotropic strain hardening. In this model, the hardening modulus was taken as 0.01 times the initial elastic modulus.

Table 4. Finite element mesh details for different regions of the model.

Modeling region	Element type	Circumferential mesh division	Longitudinal mesh division
Steel Tube Wall (CFT)	S4R	40	20
Strengthened Zone of Column	S4R	40	10
Reinforced Concrete Foundation	C3D8R	60	20
Concrete Core of Column	C3D8R	40	10

6.2. Parametric study

The conducted parametric study focused on analyzing the influence of key parameters, namely, the axial load ratio and the compressive strength of concrete, on the behavior of circular concrete-filled steel tube (CFST) composite columns. The objective of this analysis was to evaluate how these variables affect structural performance indicators, including stiffness, strength, ductility, and energy dissipation capacity.

To ensure a clear and systematic presentation, a structured specimen naming convention was adopted in this study. The format “CCFC-X-Y” was used, in which “CCFC” stands for CFST Column-to-Foundation Connection, “X” represents the axial load ratio in decimal form, and “Y” indicates the concrete compressive strength in megapascals. For instance, the specimen labeled “CCFC-0-30” refers to a CFST column-to-foundation connection with a zero axial load ratio and a concrete compressive strength of 30 MPa.

6.3. Hysteresis curve analysis

Hysteresis curves are a fundamental tool for analyzing the dynamic behavior of structures under cyclic loading, such as seismic actions. The hysteresis and backbone curves of the specimens studied in the parametric analysis are presented in Figs. 8 and 9. These curves represent the relationship between the applied lateral force and corresponding lateral displacement throughout successive

loading and unloading cycles. In the case of concrete-filled steel tube (CFST) column-to-foundation connections, hysteresis curves provide insights into stiffness, strength, ductility, and energy dissipation capacity. The shape of these curves typically reflects nonlinear behavior associated with plastic hinge formation at the column base. This nonlinear response indicates the structure's ability to undergo large deformations and absorb energy from seismic events. During the initial loading stages, the hysteresis curves exhibit steep slopes, corresponding to high initial stiffness of the connection. As lateral displacement increases, the curve slope decreases and becomes more rounded, signaling material yielding and entry into the plastic region. The hysteresis loops defined by the enclosed area between the loading and unloading paths serve as a metric for energy dissipation. With increasing displacement amplitude in each cycle, the area of these loops expands, reflecting enhanced energy absorption capacity, which is especially critical for seismic-resistant design, as energy dissipation mechanisms can help prevent structural collapse. Comparison of hysteresis curves across different specimens reveals that parameters such as embedment depth and axial load ratio significantly influence connection behavior. Greater embedment depth and higher axial load ratios (e.g., 0.3) can enhance connection stiffness and strength but may reduce ductility. Specimens subjected to higher axial loads exhibit increased load-bearing capacity; however, the hysteresis loop area at larger displacements tends to decrease, indicating reduced ductility. These findings highlight the importance of optimized design to achieve a balanced trade-off between stiffness, strength, and ductility, thereby maximizing the seismic performance of CFST connections. Table 5 summarizes the results of the parametric analysis on the seismic response of CFST column-foundation connections.

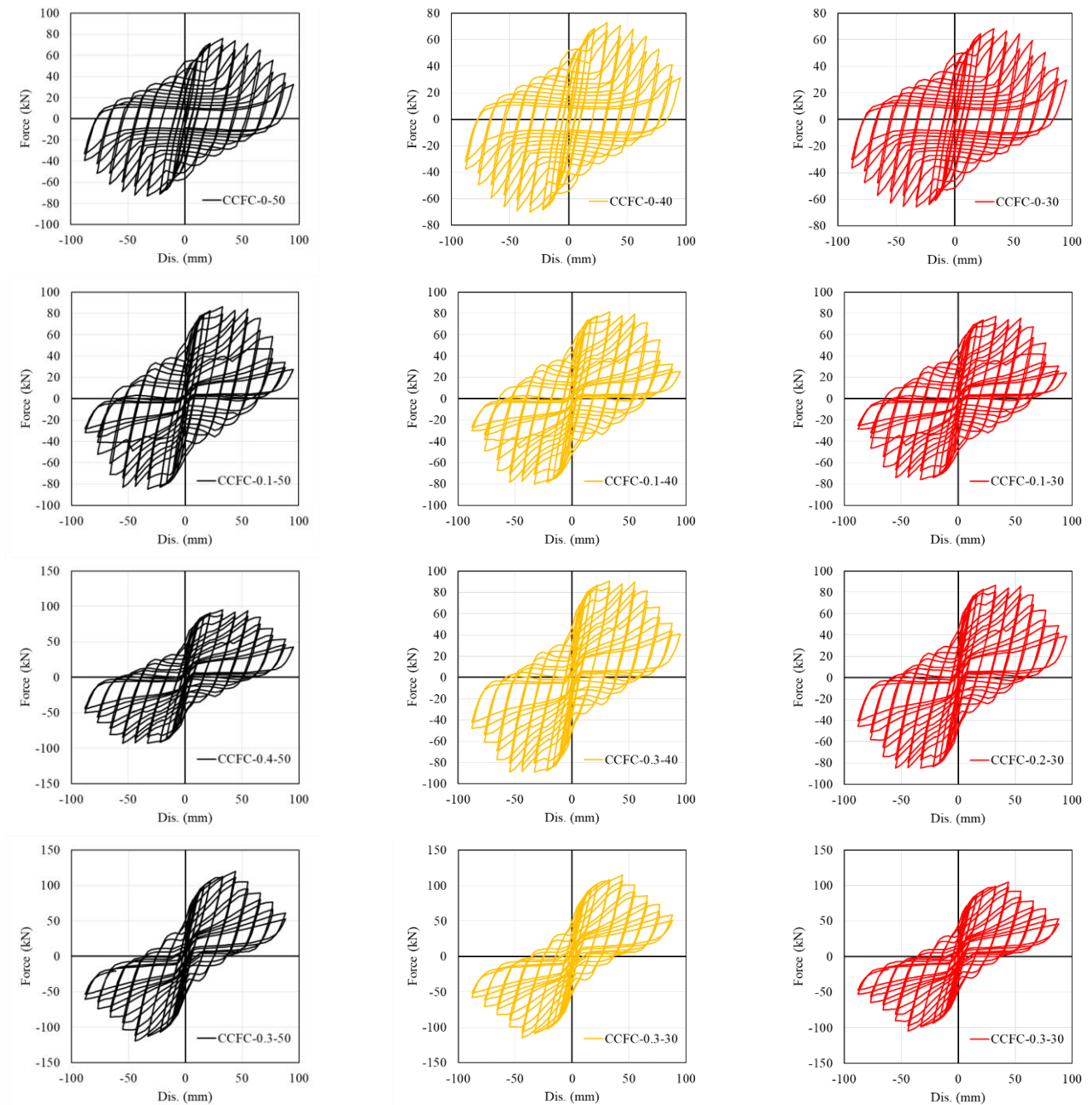


Fig. 8. Hysteresis curves of CFST column-foundation specimens in the parametric study.

6.4. Effect of concrete compressive strength

Based on the data presented in Table 6, the effect of increasing the compressive strength of concrete (30, 40, and 50 MPa) on the hysteretic performance of concrete-filled steel tube (CFST) column-to-foundation connections was examined through key parameters: secant stiffness (K), yield force (P_y), peak force (P_{max}), yield displacement (δ_y), displacement at 85% of peak capacity (δ_u), ductility (μ), and absorbed energy (E). Overall, increasing the concrete strength enhanced stiffness, strength, and energy dissipation capacity. However, its influence on ductility varied depending on the axial load ratio (0, 0.1, 0.2, and 0.3). This analysis explores the effects of concrete strength at three levels in combination with various axial load ratios. Fig. 10 illustrates how variations in concrete compressive strength affect the cyclic lateral load-displacement behavior and energy dissipation capacity of CFST column-to-foundation specimens.

At lower axial load ratios (0, 0.1, and 0.2), increasing the concrete strength from 30 MPa to 50 MPa resulted in an 8–14% improvement in K , an 11–14% increase in P_y , and an 11–14% rise in P_{max} . For instance, in specimens ranging from CCFC-0-30 to CCFC-0-50, stiffness increased from 4.06 to 4.39 kN/mm, yield force from 61.76 to 68.54 kN, and peak force from 68.27 to 75.94 kN. Additionally, the E rose notably by up to 10% demonstrating improved seismic energy dissipation. However, μ decreased with increasing concrete strength (from 4.12 to 3.85 at zero axial load), likely due to the more brittle behavior of higher-strength concrete. δ_y experienced a slight increase, while the δ_u reduced, indicating more concentrated plastic deformations.

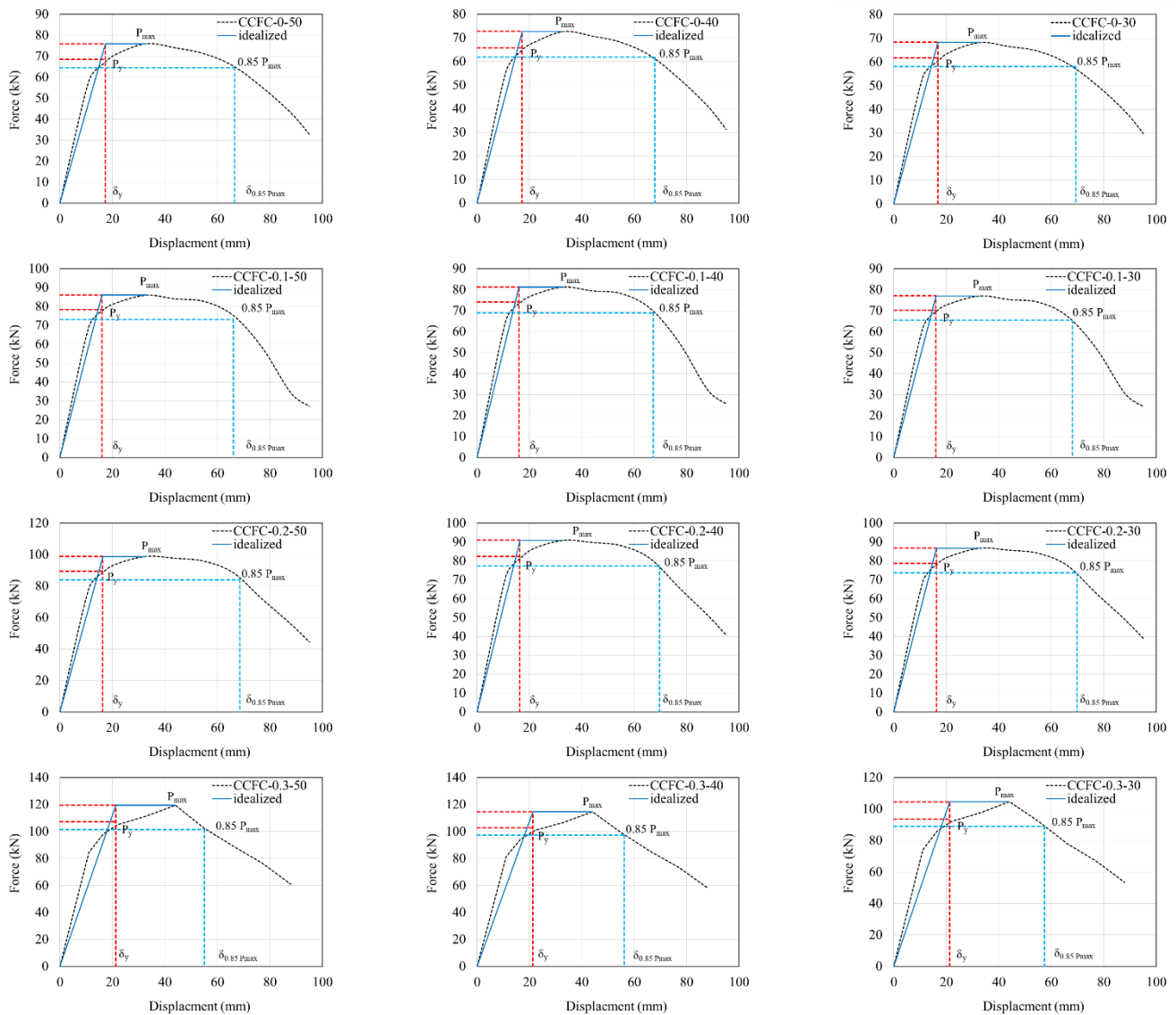


Fig. 9. Backbone curves of CFST specimens under cyclic loading in the parametric study.

At a higher axial load ratio (0.3), the influence of concrete strength on hysteresis behavior shifted. Increasing concrete strength from 30 to 50 MPa continued to enhance stiffness (from 4.93 to 5.63 kN/mm), yield force (from 93.73 to 107.39 kN), and peak force (from 104.69 to 119.60 kN). However, ductility noticeably declined (from 2.70 to 2.59). This reduction stems from the higher axial load, which induces a more brittle response due to the combined effects of compressive and flexural stresses. Although energy absorption increased by up to 14%, the hysteresis loop area at larger displacements diminished due to reduced ductility.

Table 5. Parametric study on the seismic performance indicators of CFST column-foundation connections.

Specimens	Initial stiffness K (kN/mm)	Yield load P_y (kN)	Maximum load P_{max} (kN)	Yield displacement δ_y (mm)	Ultimate displacement at 85% peak load δ_u (kN)	Ductility μ	Energy dissipation E (kN.mm)
CCFC-0-30	4.06	61.76	68.27	16.80	69.21	4.12	61797.22
CCFC-0-40	4.24	65.79	72.76	17.18	67.85	3.95	65386.92
CCFC-0-50	4.39	68.54	75.94	17.29	66.51	3.85	68244.33
CCFC-0.1-30	4.80	70.22	77.05	16.05	68.08	4.24	67779.60
CCFC-0.1-40	5.09	74.13	81.29	15.97	67.20	4.21	72496.53
CCFC-0.1-50	5.39	78.50	86.08	15.97	66.17	4.14	77234.42
CCFC-0.2-30	5.33	78.72	86.72	16.27	69.81	4.29	68918.80
CCFC-0.2-40	5.56	82.38	90.88	16.36	69.70	4.26	74128.00
CCFC-0.2-50	6.06	89.65	98.84	16.32	68.56	4.20	77634.65
CCFC-0.3-30	4.93	93.73	104.69	21.25	57.31	2.70	65599.25
CCFC-0.3-40	5.39	102.78	114.59	21.25	56.10	2.64	71841.24
CCFC-0.3-50	5.63	107.39	119.60	21.25	55.10	2.59	75065.42

These findings underscore that, in the design of CFST connections under high axial loads, any increase in concrete strength must be carefully balanced to maintain an optimal compromise between strength and ductility.

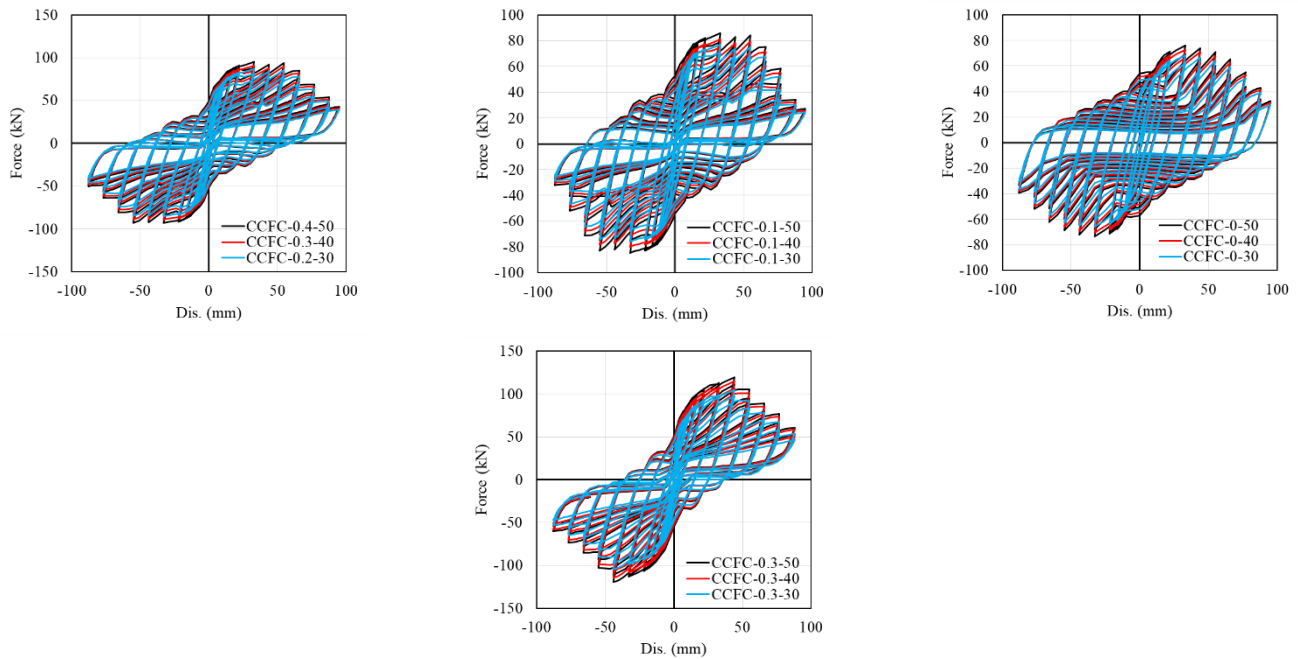


Fig. 10. Effect of concrete compressive strength on hysteresis response.

Table 6. Normalized comparison of key seismic performance indicators relative to the reference specimen (30 MPa concrete strength- $I = 30, 40, 50$).

Specimen	Stiffness ratio (K_i/K_{30})	Peak load ratio (P_i/P_{30})	Ductility ratio (μ_i/μ_{30})	Energy ratio (E_i/E_{30})
CCFC-0-30	1.00	1.00	1.00	1.00
CCFC-0-40	1.04	1.07	0.96	1.06
CCFC-0-50	1.08	1.11	0.93	1.10
CCFC-0.1-30	1.00	1.00	1.00	1.00
CCFC-0.1-40	1.06	1.06	0.99	1.07
CCFC-0.1-50	1.12	1.12	0.98	1.14
CCFC-0.2-30	1.00	1.00	1.00	1.00
CCFC-0.2-40	1.04	1.05	0.99	1.08
CCFC-0.2-50	1.14	1.14	0.98	1.13
CCFC-0.3-30	1.00	1.00	1.00	1.00
CCFC-0.3-40	1.09	1.09	0.98	1.10
CCFC-0.3-50	1.14	1.14	0.96	1.14

6.5. Effect of axial load

In the present parametric study, the influence of varying axial load ratios (0, 0.1, 0.2, and 0.3) on the hysteretic behavior of concrete-filled steel tube (CFST) column-to-foundation connections was evaluated. Hysteresis behavior, analyzed through load-displacement curves under cyclic loading, reflects key structural performance indices including K , P_y , P_{max} , δ_y , δ_u , μ , and E . The tabulated data indicate that increasing axial load ratio, particularly in the range of 0 to 0.3, leads to significant changes in these indicators. The influence of axial load ratio on the cyclic performance of CFST column-to-foundation connections is observed in Fig. 11. Corresponding normalized performance parameters, including stiffness, peak load, ductility, and energy dissipation, are presented in Table 7.

An increase in axial load ratio from 0 to 0.3 generally improves K , P_y , and P_{max} . For example, in specimens with a concrete compressive strength of 30 MPa, secant stiffness increased from 4.06 kN/mm in CCFC-0-30 to 4.93 kN/mm in CCFC-0.3-30, while peak force rose from 68.27 kN to 104.69 kN. However, this enhancement in axial load is accompanied by a notable reduction in μ , decreasing from 4.12 in CCFC-0-30 to 2.70 in CCFC-0.3-30. This decline signifies a restriction in the plastic deformation capacity of the connection under higher axial loads.

On the other hand, E tends to increase with axial load in most cases, particularly in specimen CCFC-0.2-50, which reached 77,634.65 kN-mm. However, at an axial load ratio of 0.3, the rise in energy absorption becomes more limited due to diminished ductility. These observations demonstrate that while higher axial loads enhance stiffness and strength, they may negatively affect ductility and plastic performance, highlighting the need for a carefully balanced design in seismic applications.

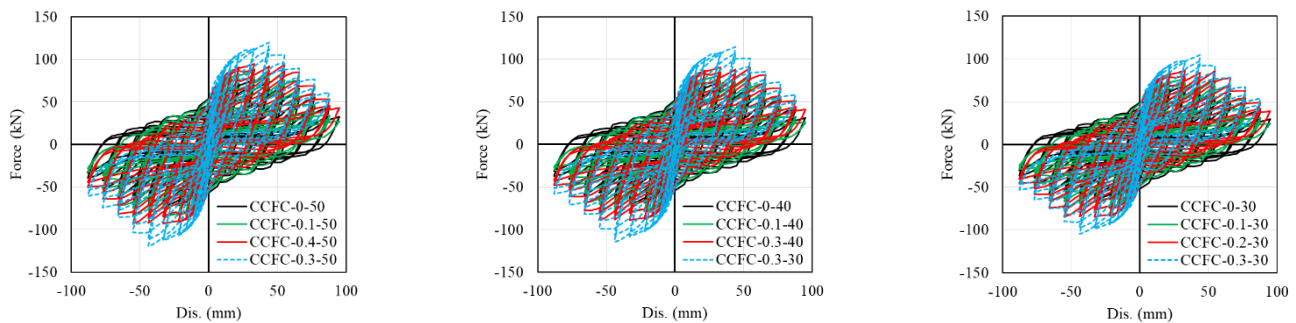


Fig. 11. Effect of axial load ratio on hysteretic behavior of CFST specimens.

The results for the 30 MPa concrete strength group illustrate the impact of increasing axial load ratios (0, 0.1, 0.2, and 0.3) on the hysteretic behavior of CFST column-to-foundation connections. As axial load increased, secant stiffness rose by up to 31.28% (from 4.06 to 5.33 kN/mm), and peak load improved by 53.35% (from 68.27 to 104.69 kN), indicating a substantial enhancement in load-carrying capacity and resistance to initial deformations. However, ductility at an axial load ratio of 0.3 dropped by 34.47% (from 4.12 to 2.70), reflecting a restriction in plastic deformation capacity and a reduced ability to accommodate large displacements. Absorbed energy increased by up to 11.50%, although this gain was more limited at higher axial load ratios due to reduced ductility. These findings highlight the importance of optimizing axial load to maintain a balanced performance in terms of stiffness, strength, and ductility for seismic design.

The specimens with 40 MPa concrete exhibited consistent behavioral trends as the axial load ratio increased from 0 to 0.3. Secant stiffness improved by up to 31.13% (from 4.24 to 5.56 kN/mm), and peak load increased by 57.52% (from 72.76 to 114.59 kN), emphasizing enhanced interaction between the steel tube and concrete infill. However, ductility dropped by 33.16% (from 3.95 to 2.64), accompanied by a 23.69% rise in yield displacement and a 17.32% reduction in the 85% capacity displacement—signifying more concentrated deformation zones. Energy absorption increased by 13.37%, but the observed reduction in ductility under higher axial loads again highlights the need for design caution to preserve plastic deformation capacity, especially in seismic applications.

In the 50 MPa concrete strength group, axial load increases led to even more pronounced gains: secant stiffness rose by 38.04% (from 4.39 to 6.06 kN/mm), and peak load increased by 57.49% (from 75.94 to 119.60 kN), signifying marked improvements in structural performance. However, ductility declined by 32.73% (from 3.85 to 2.59) at an axial load ratio of 0.3, indicating increased brittleness and reduced deformation capacity. While absorbed energy increased by up to 13.67%—the highest among the tested concrete strengths—this gain became limited under high axial load due to constrained ductility. These observations emphasize the necessity of carefully calibrating design parameters to balance stiffness and ductility under seismic loading, particularly when using high-strength concrete with elevated stiffness and strength potential.

6.6. Analysis of dissipated energy variations

The analysis E in concrete-filled steel tube (CFST) column-to-foundation connections, based on tabulated data, illustrates the effects of axial load ratio (0, 0.1, 0.2, and 0.3) and concrete compressive strength (30, 40, and 50 MPa) on the seismic energy dissipation capacity. As illustrated in Fig. 12, the cumulative energy dissipation increases significantly with improvements in axial load ratio and concrete strength, while variations in embedment depth show a more moderate effect. Dissipated energy—quantified by the area enclosed within the hysteresis loops of the force–displacement curves—is a key indicator for evaluating seismic performance, as it reflects the structure's ability to dissipate cyclic energy and reduce dynamic earthquake effects. This analysis emphasizes the underlying scientific principles and engineering mechanisms influencing energy dissipation behavior.

Table 7. Parametric comparison of normalized seismic performance indicators relative to the baseline CFST specimen ($i=0, 0.1, 0.2, 0.3$).

Specimen	Stiffness ratio (K_i/K_0)	Peak load ratio (P_i/P_0)	Ductility ratio (μ_i/μ_0)	Energy ratio (E_i/E_0)
CCFC-0-30	1.00	1.00	1.00	1.00
CCFC-0.1-30	1.18	1.13	1.03	1.10
CCFC-0.2-30	1.31	1.27	1.04	1.12
CCFC-0.3-30	1.21	1.53	0.65	1.06
CCFC-0-40	1.00	1.00	1.00	1.00
CCFC-0.1-40	1.20	1.12	1.07	1.11
CCFC-0.2-40	1.31	1.25	1.08	1.13
CCFC-0.3-40	1.27	1.57	0.67	1.10
CCFC-0-50	1.00	1.00	1.00	1.00
CCFC-0.1-50	1.23	1.13	1.08	1.13
CCFC-0.2-50	1.38	1.30	1.09	1.14
CCFC-0.3-50	1.28	1.57	0.67	1.10

For 30 MPa concrete, dissipated energy increased from 61,797.22 to 68,918.80 kN·mm (an 11.50% rise) as the axial load ratio increased from 0 to 0.2. This improvement stems from enhanced interaction between the steel tube and the concrete core due to higher compressive stress, which leads to increased stiffness (up to 31.28%) and strength (up to 27.00%), thereby enlarging the hysteresis loops at intermediate displacement levels. However, at an axial load ratio of 0.3, energy decreased to 65,599.25 kN·mm (a lower 6.15% increase), primarily due to a 34.47% drop in ductility, where local buckling of the steel tube and crushing of the concrete core limited the energy dissipation at larger deformations.

For 40 MPa concrete, dissipated energy grew from 65,386.92 to 74,128.00 kN·mm (an increase of 13.37%) at an axial load ratio of 0.2, driven by enhanced shear resistance of concrete and a 31.13% gain in stiffness. However, at a ratio of 0.3, energy only rose to 71,841.24 kN·mm (9.85% increase), as ductility declined by 33.16% and excessive compressive stress induced more brittle behavior.

With 50 MPa concrete, the highest dissipated energy was observed at a 0.2 axial load ratio, 77,634.65 kN·mm (13.67% increase), thanks to the superior compressive strength and enhanced confinement provided by the steel tube. At a ratio of 0.3, energy decreased to 75,065.42 kN·mm (a 9.98% rise), with ductility dropping by 32.73% due to premature crushing of the concrete core under elevated compressive stresses, thereby limiting hysteresis loop expansion.

From a scientific and engineering standpoint, increasing the axial load ratio up to 0.2 improves confinement and enhances energy dissipation capacity. However, at 0.3, excessive axial stress accelerates local buckling and suppresses plastic behavior. Therefore, for seismic design of CFST connections, an axial load ratio of 0.2 is considered optimal to ensure a balanced performance between dissipated energy, stiffness, and ductility. Higher load ratios may require additional confinement or reinforcement strategies to prevent premature failure.

6.7. Analysis of axial and hoop strain variations at the column base

The variations in axial and hoop strains at the base of concrete-filled steel tube (CFST) columns connected to foundations are significantly influenced by the compressive strength of concrete (30, 40, and 50 MPa) and axial load ratios (0, 0.1, 0.2, and 0.3). As shown in Fig. 13, strain gauges were installed at the base of the CFST column near the column-foundation interface to monitor localized behavior. Fig. 14 presents the longitudinal load-strain response under cyclic loading, demonstrating the effects of concrete compressive strength at varying axial load ratios ($n = 0$ to 0.3). Axial strains mainly caused by compressive stresses from axial loading and flexural effects from cyclic excitation are concentrated at the column base, a critical region near the foundation. As the axial load ratio increases from 0 to 0.3, axial strains grow due to elevated compressive stresses in both the steel tube and the concrete core. This phenomenon is particularly amplified at 0.2 and 0.3 load ratios, where plastic hinge formation occurs at approximately 25–75 mm above the foundation surface. For 30 MPa concrete, increasing axial load to 0.2 enhances stiffness by 31.28% and dissipated energy by 11.50%, suggesting a favorable balance between axial strain and effective confinement. The hoop strains, resulting from the lateral pressure of the steel tube against the concrete core, help enhance ductile behavior in this range by delaying concrete cracking and increasing the plastic deformation capacity. This behavior is confirmed by higher ductility ($\mu = 4.29$ in CCFC-0.2-30) and larger hysteresis loops in the analyses. For higher-strength concrete (40 and 50 MPa), axial and hoop strain behavior under varying axial loads differs noticeably. At 40 MPa, raising the axial load to 0.2 improves stiffness (by 31.13%) and energy dissipation (by 13.37%), reflecting better confinement and reduced detrimental hoop strain. This is attributed to the concrete's enhanced capacity to withstand compressive stresses, which allows more uniform distribution of axial strains in the plastic zone and mitigates premature failure. However, at a 0.3 load ratio, axial strains become excessively exacerbated by a 23.69% increase in yield displacement while hoop strains lead to local buckling of the tube and concrete crushing under high stresses. These effects correspond to reduced ductility (by 33.16% in CCFC-0.3-40) and smaller hysteresis loops. A similar trend is observed for 50 MPa concrete, though performance metrics at a 0.2 load ratio show further improvements in stiffness, increasing by 38.04% and energy dissipation by 13.67% due to enhanced confinement. This controls hoop strain within an optimal range and promotes ductile

behavior. Nevertheless, at a 0.3 axial load ratio, excessive axial strains and a 32.73% drop in ductility indicate greater brittleness and reduced plastic capacity.

At a 0.3 load ratio across all three concrete strengths, axial strains reach critical levels that accelerate concrete crushing and tube buckling, evidenced by a 17.32% reduction in ultimate displacement and up to 34.47% loss in ductility. In this state, hoop strains exceed optimal confinement thresholds, contributing to cracking and diminished energy dissipation capacity. Although the impact is less severe in 50 MPa concrete due to its higher compressive resistance, a notable ductility loss is still observed. From an engineering perspective, these observations suggest that an axial load ratio of 0.2 provides the optimal balance between axial and hoop strain behavior for all examined concrete strengths, resulting in maximum energy dissipation and sustained ductility. For seismic design, axial load ratios beyond 0.2 are discouraged unless additional confinement measures such as thicker steel tubes or external ring stiffeners are implemented to mitigate the adverse effects of excessive strain concentrations at the column base.

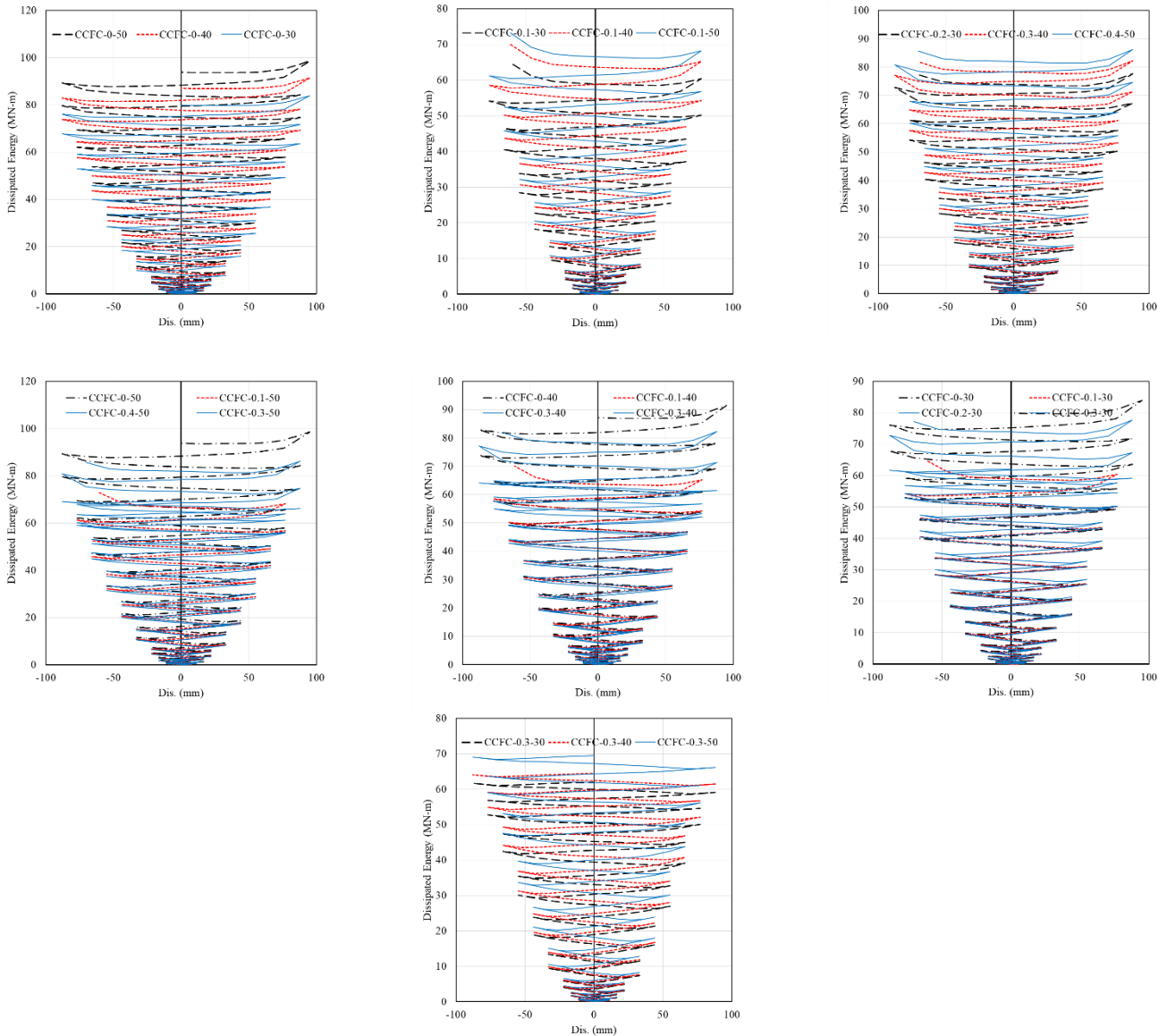


Fig. 12. Comparison of energy dissipation versus lateral displacement for various CFST column-foundation specimens.

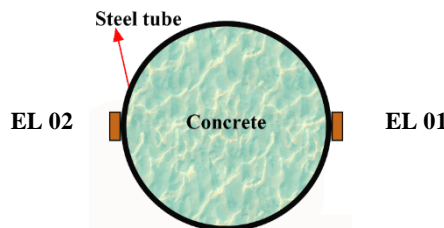


Fig. 13. Strain gauge locations at the base of the CFST column near the column-to-foundation interface.

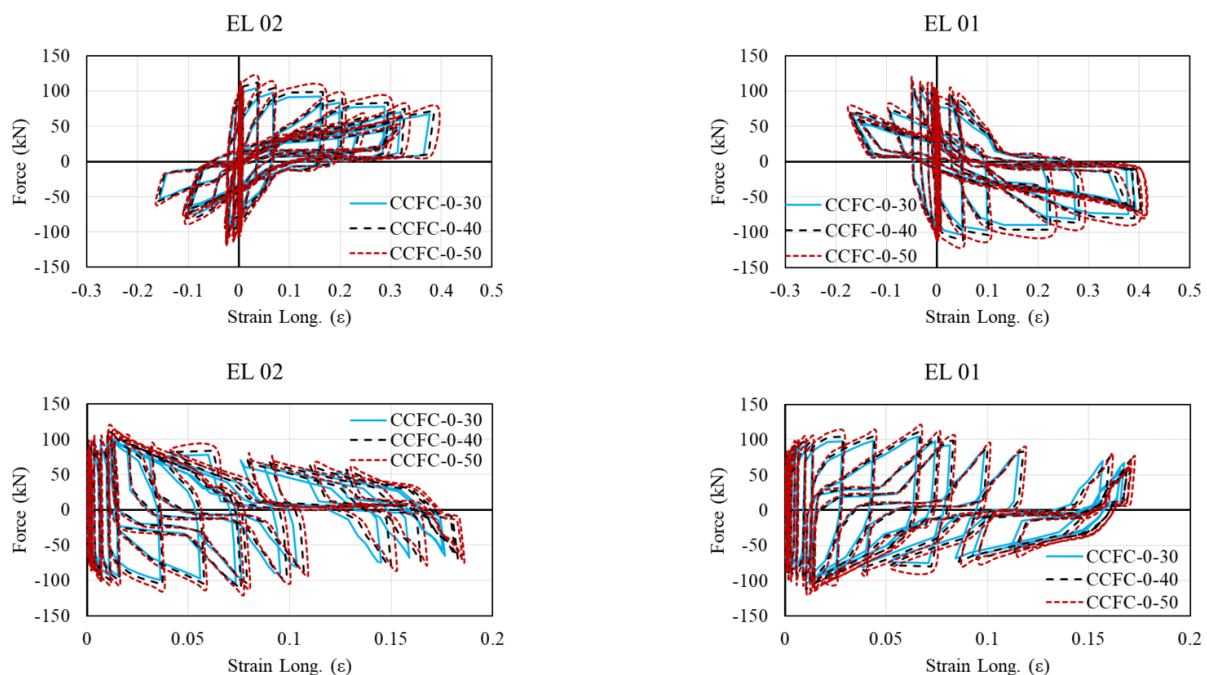
7. Conclusion

Embedded connections between circular CFST columns and foundations exhibit robust performance under cyclic loading, making them a reliable structural solution with practical construction benefits. In this study, the cyclic behavior of such connections

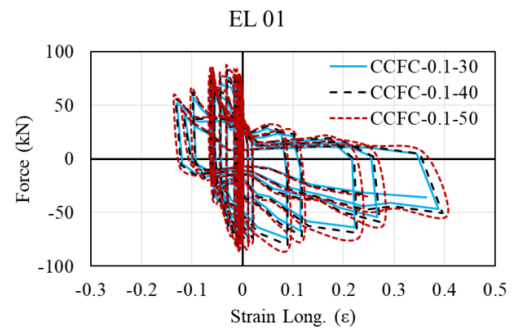
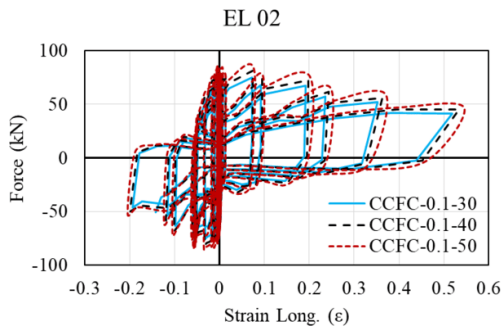
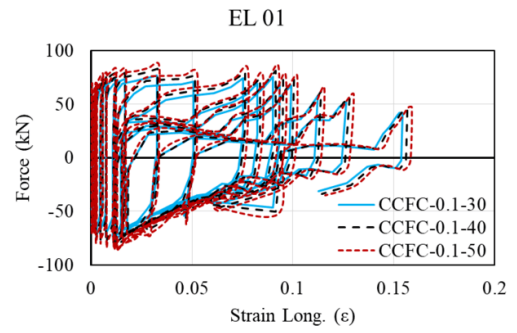
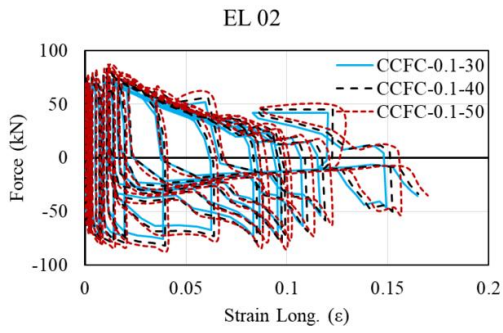
was evaluated through experimental testing and numerical simulation. The principal findings and conclusions are summarized as follows:

- The embedded connection effectively transfers both axial and lateral loads from the CFST column to the foundation while accommodating nonlinear deformations under severe loading. The dominant failure mechanism was plastic hinge formation at the column base. No signs of pull-out or brittle fracture at the interface were observed, confirming the connection's seismic reliability and ductility.
- The embedment depth (L_e) was identified as the most influential parameter affecting connection behavior. Increasing L_e led to improvements in flexural strength, energy dissipation capacity, and ductility. An embedment depth equal to the column diameter (D) was sufficient for full moment transfer and stable cyclic behavior; however, increasing the depth to $1.2D$ or beyond further enhanced hysteretic performance and mitigated stiffness degradation under large deformations.
- Due to the circular geometry of the column and the confining effect of the surrounding foundation concrete, a quasi-triaxial compressive state developed at the interface. This confinement enhanced the mechanical interlock between the steel tube and concrete core, preventing premature crushing and localized failure.
- The numerical simulations supported the experimental trends and provided valuable insights into stress distribution, confinement effects, and shear transfer mechanisms at the connection. The results highlighted that increased side friction and contact area between the column and foundation significantly enhance initial stiffness and post-yield strength.
- To ensure plastic hinge formation occurs within the column rather than at the connection, a minimum embedment depth based on internal force equilibrium and shear stress distribution is recommended. Additionally, a design expression for the minimum concrete thickness beneath the embedded region is proposed to prevent punching shear failure.
- Axial and hoop strain analyses at the base of CFST columns revealed that concrete compressive strength (30, 40, and 50 MPa) and axial load ratio (0, 0.1, 0.2, and 0.3) significantly influence seismic performance. Increasing axial load up to 0.2, particularly with 50 MPa concrete, enhanced stiffness (by up to 38.04%), strength (up to 57.49%), and energy dissipation (up to 13.67%) due to improved confinement and favorable strain distribution. However, at an axial load ratio of 0.3, excessive axial and hoop strains triggered local buckling and concrete crushing, leading to reduced ductility (up to 34.47%) and limited energy dissipation capacity.
- These findings, confirmed through ABAQUS simulations and experimental observations, underscore the importance of optimizing the axial load ratio within the range of 0.1 to 0.2 to achieve a balanced design in terms of stiffness, strength, and ductility. For seismic applications, it is recommended that CFST connections be reinforced, e.g., via increased tube thickness or ring stiffeners at the column base to mitigate the adverse effects of excessive strains under high axial load and ensure optimal structural performance.

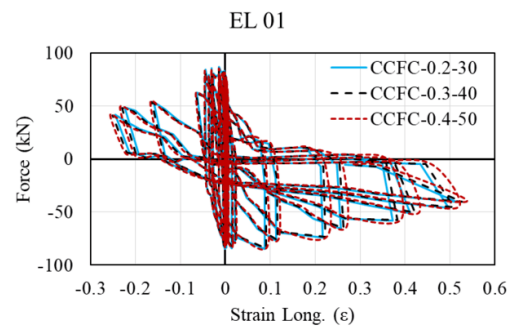
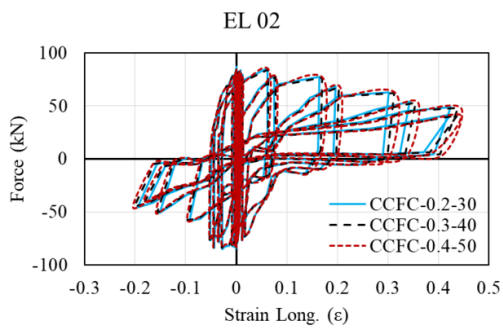
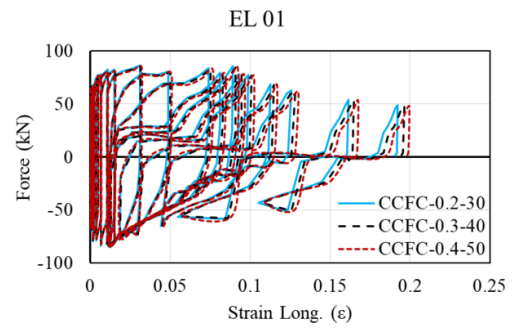
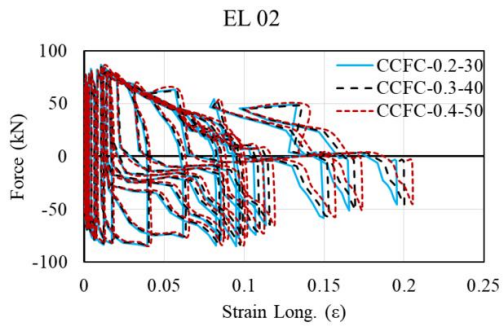
Critically, embedment depth (L_e), particularly at or beyond the column diameter (D), significantly enhances hysteretic performance, while optimal concrete compressive strength and axial load ratios (0.1-0.2) boost stiffness, strength, and energy dissipation by promoting favorable stress distribution and confinement within the composite section. Conversely, excessive axial load (0.3) can severely compromise ductility due to premature buckling and concrete crushing, underscoring the necessity for balanced design and localized reinforcement.



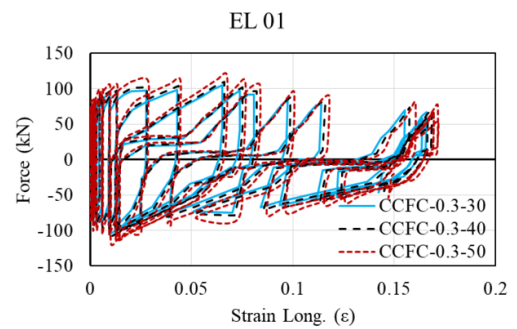
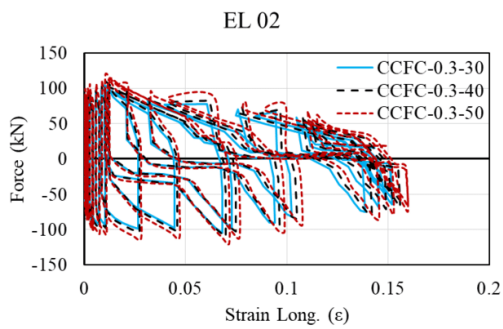
(a) Effect of concrete compressive strength ($n = 0$)



(b) Effect of concrete compressive strength (n = 0.1)



(c) Effect of concrete compressive strength (n=0.2)



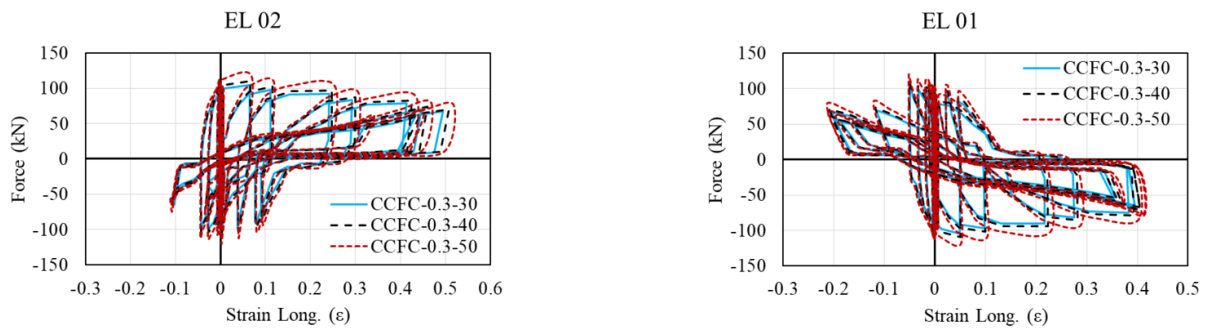
(d) Effect of concrete compressive strength ($n = 0.3$)

Fig. 14. Longitudinal load–strain response of CFST column–foundation connections under cyclic loading.

Statements & Declarations

Author contributions

Saleh Mohammad-Ebrahimzadeh-Sepasgozar: Conceptualization, Investigation, Methodology, Formal analysis, Resources, Writing - Original Draft, Writing - Review & Editing.

Morteza Naghipour: Conceptualization, Methodology, Formal analysis, Project administration, Supervision, Writing - Review & Editing.

Funding

The authors received no financial support for the research, authorship, and/or publication of this article.

Data availability

The data presented in this study will be available on interested request from the corresponding author.

Declarations

The authors declare no conflict of interest.

References

- [1] He, J. C. W., Clifton, G. C., Ramhormozian, S., Hogan, L. S. Numerical and analytical study of pinned column base plate connections. *Journal of Constructional Steel Research*, 2023; 204: 107846. doi:10.1016/j.jcsr.2023.107846.
- [2] Nawar, M. T., Matar, E. B., Maaly, H. M., Alaaser, A. G., El-Zohairy, A. Assessment of Rotational Stiffness for Metallic Hinged Base Plates under Axial Loads and Moments. *Buildings*, 2021; 11: doi:10.3390/buildings11080368.
- [3] Khodaie, S., Mohamadi-shooreh, M. R., Mofid, M. Parametric analyses on the initial stiffness of the SHS column base plate connections using FEM. *Engineering Structures*, 2012; 34: 363-370. doi:10.1016/j.engstruct.2011.09.026.
- [4] Grauvilardell, J. E., Lee, D. Synthesis of Design, Testing and Analysis Research on Steel Column Base Plate Connections in High-Seismic Zones. Minneapolis (MN): Department of Civil Engineering, University of Minnesota; 2005. Report No.: ST-04-02.
- [5] Camacho, J. Seismic performance of exposed column base plates (Phase I). In: 2007 Earthquake Engineering Symposium for Young Researchers, Multi-Disciplinary Center for Earthquake Engineering Research (MCEER); 2007 Nov 1; Buffalo, United States. p. 52-69.
- [6] Abejide, O. S. Effectiveness of Base Plate Thickness Design Criteria in Steel Columns. *Research Journal of Applied Sciences*, 2007; 2: 1207-1217. doi:rjasci.2007.1207.1217.
- [7] Kanvinde, A. M., Jordan, S. J., Cooke, R. J. Exposed column base plate connections in moment frames — Simulations and behavioral insights. *Journal of Constructional Steel Research*, 2013; 84: 82-93. doi:10.1016/j.jcsr.2013.02.015.
- [8] Hitaka, T., Suita, K., Kato, M. CFT column base design and practice in Japan. In: Proceedings of the International Workshop on Steel and Concrete Composite Construction; 2003 Oct 1; p. 8-9.
- [9] Hitaka, T., Matsui, C., Sakai, J. i. Cyclic tests on steel and concrete-filled tube frames with Slit Walls. *Earthquake Engineering & Structural Dynamics*, 2007; 36: 707-727. doi:10.1002/eqe.648.
- [10] Marson, J., Bruneau, M. Cyclic Testing of Concrete-Filled Circular Steel Bridge Piers having Encased Fixed-Based Detail. *Journal of Bridge Engineering*, 2004; 9: 14-23. doi:10.1061/(ASCE)1084-0702(2004)9:1(14).
- [11] Zhang, G., Xiao, Y., Kunnath, S. Low-Cycle Fatigue Damage of Circular Concrete-Filled-Tube Columns. *ACI Structural Journal*, 2009; 106: doi:10.14359/56353.

- [12] Roeder Charles, W., Lehman Dawn, E., Bishop, E. Strength and Stiffness of Circular Concrete-Filled Tubes. *Journal of Structural Engineering*, 2010; 136: 1545-1553. doi:10.1061/(ASCE)ST.1943-541X.0000263.
- [13] Moon, J., Roeder, C. W., Lehman, D. E., Lee, H.-E. Analytical modeling of bending of circular concrete-filled steel tubes. *Engineering Structures*, 2012; 42: 349-361. doi:10.1016/j.engstruct.2012.04.028.
- [14] Moon, J., Lehman Dawn, E., Roeder Charles, W., Lee, H.-E. Strength of Circular Concrete-Filled Tubes with and without Internal Reinforcement under Combined Loading. *Journal of Structural Engineering*, 2013; 139: 04013012. doi:10.1061/(ASCE)ST.1943-541X.0000788.
- [15] Moon, J., Lehman, D. E., Roeder, C. W., Lee, H.-E. Evaluation of embedded concrete-filled tube (CFT) column-to-foundation connections. *Engineering Structures*, 2013; 56: 22-35. doi:10.1016/j.engstruct.2013.04.011.
- [16] Lee, S.-S., Moon, J., Park, K.-S., Bae, K.-W. Strength of Footing with Punching Shear Preventers. *The Scientific World Journal*, 2014; 2014: 474728. doi:10.1155/2014/474728.
- [17] Moon, J., Lehman, D. E., Roeder, C. W., Lee, H.-E., Lee, T.-H. Analytical Evaluation of Reinforced Concrete Pier and Cast-in-Steel-Shell Pile Connection Behavior considering Steel-Concrete Interface. *Advances in Materials Science and Engineering*, 2016; 2016: 4159619. doi:10.1155/2016/4159619.
- [18] Building and Housing Research Center. Part 10: National Building Regulations of Iran – Part 10: Steel Structures. Tehran (IR): Ministry of Roads and Urban Development; 2024 (In Persian).
- [19] Kenarangi, H., Bruneau, M. Experimental Study on Composite Action in Reinforced Concrete-Filled Steel-Tube Shaft Foundations. *Journal of Bridge Engineering*, 2019; 24: 04019060. doi:10.1061/(ASCE)BE.1943-5592.0001407.
- [20] Liu, J., Xu, T., Wang, X. Seismic Behavior and Design of Concrete-Filled Thin-Walled Steel Tube Column-to-Foundation Connections. *Journal of Structural Engineering*, 2021; 147: 04021072. doi:10.1061/(ASCE)ST.1943-541X.0003037.
- [21] Xu, T., Zhang, S., Liu, J., Wang, X., Guo, Y. Seismic behavior of carbon fiber reinforced polymer confined concrete filled thin-walled steel tube column-foundation connection. *Composite Structures*, 2022; 279: 114804. doi:10.1016/j.compstruct.2021.114804.
- [22] Chen, Z., Xu, J., Zhou, T., Su, J. Seismic research on column base joint of L-shaped CFST columns under cyclic loading. *Structures*, 2022; 45: 1212-1224. doi:10.1016/j.istruc.2022.09.095.
- [23] Zhou, X., Xu, T., Liu, J., Wang, X., Chen, Y. F. Seismic performance of concrete-encased column connections for concrete filled thin-walled steel tube piers. *Engineering Structures*, 2022; 269: 114803. doi:10.1016/j.engstruct.2022.114803.
- [24] Di, J., Han, B., Zhou, X., Hu, L., Qi, Y., Qin, F. Experimental investigation into cyclic working performances of prefabricated CFST columns with improved column-footing connections. *Journal of Building Engineering*, 2022; 46: 103772. doi:10.1016/j.jobe.2021.103772.
- [25] Benjamin L. Worsfold, J. P. M., John, F. S. Moment Transfer at Column-Foundation Connections: Physical Tests. *ACI Structural Journal*, 119: doi:10.14359/51734799.
- [26] Liu, B., Zhang, L., Sun, H., Feng, M., Dou, K. Side shear strength and load-transfer mechanism of corrugated steel column–foundation socket connection. *Case Studies in Construction Materials*, 2022; 17: e01377. doi:10.1016/j.cscm.2022.e01377.
- [27] Cogurcu, M. T., Uzun, M. Experimental investigation of a new precast column-foundation connection under cyclic loading. *Journal of Building Engineering*, 2022; 50: 104245. doi:10.1016/j.jobe.2022.104245.
- [28] Haraldsson Olafur, S., Janes Todd, M., Eberhard Marc, O., Stanton John, F. Seismic Resistance of Socket Connection between Footing and Precast Column. *Journal of Bridge Engineering*, 2013; 18: 910-919. doi:10.1061/(ASCE)BE.1943-5592.0000413.
- [29] Mohebbi, A., Saiidi, M. S., Itani Ahmad, M. Shake Table Studies and Analysis of a PT-UHPC Bridge Column with Pocket Connection. *Journal of Structural Engineering*, 2018; 144: 04018021. doi:10.1061/(ASCE)ST.1943-541X.0001997.
- [30] Wang, Z., Li, T., Qu, H., Wei, H., Li, Y. Seismic Performance of Precast Bridge Columns with Socket and Pocket Connections Based on Quasi-Static Cyclic Tests: Experimental and Numerical Study. *Journal of Bridge Engineering*, 2019; 24: 04019105. doi:10.1061/(ASCE)BE.1943-5592.0001463.
- [31] Zhang, G., Han, Q., Xu, K., Du, X., He, W. Experimental investigation of seismic behavior of UHPC-filled socket precast bridge column-foundation connection with shear keys. *Engineering Structures*, 2021; 228: 111527. doi:10.1016/j.engstruct.2020.111527.
- [32] Si, X., Wen, J., Zhang, G., Jia, Z., Han, Q. Seismic performance of precast double-column pier with UHPC-filled socket connections. *Engineering Structures*, 2023; 285: 115618. doi:10.1016/j.engstruct.2023.115618.
- [33] Zhang, G., Han, Q., Xu, K., Song, Y., Li, J., He, W. Numerical analysis and design method of UHPC grouted RC column- footing socket joints. *Engineering Structures*, 2023; 281: 115755. doi:10.1016/j.engstruct.2023.115755.
- [34] American Concrete Institute (ACI). ACI 318-19: Building Code Requirements for Structural Concrete and Commentary. Farmington Hills (MI): ACI; 2019. doi:10.14359/51716937.

- [35] American Institute of Steel Construction (AISC). AISC 360-22: Specification for Structural Steel Buildings. Farmington Hills (MI): AISC; 2022.